



In-Flight Oxidation of Aluminum in the Twin-Wire Electric Arc Process

Donna Post Guillen and Brian G. Williams

(Submitted August 25, 2005; in revised form November 30, 2005)

This paper examines the in-flight oxidation of aluminum sprayed in air using the twin-wire electric arc (TWEA) thermal spray process. Aerodynamic shear at the droplet surface increases the amount of in-flight oxidation by promoting entrainment of the surface oxides within the molten droplet and continually exposing fresh fluid available for oxidation. Mathematical predictions herein confirm experimental measurements that reveal an elevated, nearly constant surface temperature (~2273 K) of the droplets during flight. The calculated oxide volume fraction of a “typical” droplet with internal circulation compares favorably to the experimentally determined oxide content (3.3-12.7%) for a typical TWEA-sprayed aluminum coating sprayed onto a room temperature substrate. It is concluded that internal circulation within the molten aluminum droplet is a significant source of oxidation. This effect produces an oxide content nearly two orders of magnitude larger than that of a droplet without continual oxidation.

Keywords aluminum coatings, oxidation, twin-wire electric arc process

1. Introduction

The oxidation behavior of an in-flight molten aluminum droplet produced by the twin-wire electric arc (TWEA) thermal spray process is examined by comparing experimental data with theory. In-flight oxidation of aluminum droplets is accompanied by two effects: (a) a fluid dynamic effect, which promotes entrainment and mixing of the surface oxides within the droplet, and (b) a heat transfer effect, which causes an increase in droplet temperature over that of a solid particle (i.e., no internal circulation). It has been shown that the fluid dynamic effects cause a toroidal flow within the droplet (Ref 1), continually exposing fresh fluid available for oxidation. This continuous oxidation produces the effects of an elevated temperature during droplet flight to the substrate and an increase in the final oxidation percentage of a typical coating, as compared with a droplet without internal circulation.

2. Description of a “Typical” Droplet

A Praxair Tafa Inc. (Concord, NH) Model 9000 TWEA spray system was operated at a voltage of 28 V with spray gun amperage and pressure settings varied from 100 to 300 A and 40 to 75 psi, respectively. Praxair Tafa 01T aluminum wire (1/16 in. [1.59 mm] diameter) was sprayed in air using a spray gun equipped with a blue nozzle cap (0.375 in. [9.525 mm] orifice) and a short-cross wire positioner. Real-time, nonintrusive spray plume data obtained using phase Doppler anemometry, in-flight particle pyrometry, and Pitot tube measurements were used as the basis for

defining a “typical” droplet. These experiments, described in detail in Ref 2, yielded average diameter, velocity, and temperature of the melted, atomized droplets, along with relative droplet number density and air stream velocity data. The data show that the aluminum droplets remain in a liquid state throughout their flight to the substrate, as the temperatures are well above the melting temperature (933 K) yet below the boiling point (2723 K) (Ref 3).

The goal of this analysis is to devise a model that is simple, yet accurate enough to make valid predictions of the underlying physical processes. A “typical” droplet in the spray plume is defined as a 39 μm aluminum droplet traveling through air at 164 m s^{-1} with a mean relative velocity of 140 m s^{-1} , a temperature of 2273 K, and a Reynolds number (based on diameter) of 300. These values were obtained by averaging the experimentally measured data for the 100 A/75 psi setting along the plume centerline from the gun exit to 178 mm. The relative droplet number density data show that the highest concentration of droplets is along the plume centerline, therefore this region contains the droplets that make up the bulk of the coating. The “typical” droplet temperature was used only to specify material properties for the calculations.

3. Aluminum Oxidation Reaction

Aluminum is a reactive metal with a strong affinity for oxygen (Ref 4). The oxidation reaction is highly exothermic and the small droplet sizes offer a large surface area to volume ratio available for oxidation. Electrons pass from the metal via the quantum mechanical tunnel effect to the oxygen adsorbed on the surface of the film. Cations form at the metal-oxide interface and oxygen anions form at the oxide-air interface. The strong electric field established across the thin oxide film pulls the ions through the film (Ref 5). In-flight oxidation of a “typical” droplet occurs during the time ($t_s = 1.08$ ms) when the droplet travels from its origin at the wire tips ($x = 0.84$ mm) to the substrate location ($x = 178$ mm). For very short times (i.e., much less than

Donna Post Guillen, Idaho National Laboratory, Idaho Falls, ID; and Brian G. Williams, Idaho State University, Pocatello, ID. Contact e-mail: Donna.Guillen@inl.gov.

several minutes [Ref 6]), a thin oxide film is formed that obeys a linear rate law. On the basis of the theory established by Cabrera and Mott (Ref 7), Dai et al. (Ref 8) expressed the growth of the oxide layer as:

$$\frac{d\delta}{dt} = 2A_0 \exp\left(-\frac{Q_e}{k_b T_d}\right) \exp\left(k_e \frac{P_{O_2}^{1/2}}{k_b T_d}\right) \quad (\text{Eq 1})$$

where the oxidation equation constants for aluminum were determined experimentally as $A_0 = 2.5 \times 10^6 \text{ \AA s}^{-1}$, $Q_e = 1.6 \text{ eV}$, $k_e = 0.139 \text{ eV/torr}$, and k_b is Boltzmann's constant (J K^{-1}), T_d is

droplet temperature (K), and P_{O_2} is the oxygen partial pressure (torr). From Eq 1, the rate of oxide growth is more sensitive to the oxygen content of the atomizing air stream than to droplet temperature.

As the airflow exits the nozzle, the pressure in the jet adjusts through a series of expansions and shocks until it reaches the ambient pressure. In reality, the pressure distribution around the droplet varies, but for the purposes of this analysis it is approximated as a constant value (i.e., the ambient atmospheric pressure). The atmospheric pressure at the laboratory altitude of 4500 ft (1372 m) during the acquisition of in-flight droplet data was 12.43 psia (Ref 2). Because standard air is composed of 20.95 vol.% oxygen, the partial pressure of oxygen in air, P_{O_2} , is 134 torr. Using Eq 1, the estimated rate of growth of the surface oxide layer during droplet flight for a "typical" droplet is $5.24 \times 10^{-4} \text{ m s}^{-1}$.

4. Fluid Dynamic Effect

It is well known that aerodynamic shear induces internal circulation in droplets, such as fuel sprays and raindrops (Ref 1). The resulting convective effect within a liquid droplet, also known as Hill's spherical vortex, was described over a century ago (Ref 9). Such convective motions were also described by Batchelor (Ref 10), Harper and Moore (Ref 11), and Prakash and Sirignano (Ref 12). LeClair et al. (Ref 13) observed flow patterns within a water droplet falling at terminal velocity in air by experiments performed in a wind tunnel where the water droplets were seeded with carbon or aluminum tracer particles and the internal circulation was recorded using streak photography. More recently, Melton (Ref 14) used droplet exciplex (e.g., excited complex) fluorescence to experimentally verify internal circulation in liquid droplets. The existence of such phenomena in droplets produced by thermal spray processes was suggested by Neiser et al. (Ref 15).

The presence of a two-dimensional toroidal flow field within a molten aluminum droplet produced by TWEA spraying is stimulated by shear forces due to high-velocity airflow around the droplet (Fig. 1). Sirignano (Ref 1) describes four major regions of flow around and within a liquid droplet in a spray. Region 1 is the inviscid freestream airflow over the droplet far away from the air-droplet interface and outside the wake. Region 2 includes the viscous boundary layer external to the droplet and the near wake. Region 3 contains the liquid internal boundary layer and wake (e.g., region along the axis of symmetry through which the liquid circulating out of the boundary layer passes). Region 4 consists of the rotational, nearly shear free flow that comprises the toroidal core and can be described by Hill's spherical vortex.

The liquid motion of the in-flight molten aluminum droplets in the TWEA spray process continually sweeps fresh fluid to the surface of the droplet where it then oxidizes. The oxidation reaction occurs as long as there is a velocity difference between the liquid droplet and the freestream air, which creates aerodynamic shear and drives the internal circulation inside the droplet. In the following subsections, it will be shown that the sustained high droplet temperatures that keep the droplet in a liquid state are caused by continual oxidation reaction of the molten aluminum with air. The oxide that forms at the droplet surface is entrained

Nomenclature		
A	droplet surface area	m^2
A_0	coefficient in Eq 1	\AA s^{-1}
A_{ox}	oxidation area	m^2
Bi	Biot number	
c_p	specific heat at constant pressure	$\text{J kg}^{-1} \text{K}^{-1}$
D	droplet diameter	μm
\dot{E}_{in}	rate of energy entering the system through the control volume	W
\dot{E}_{g}	rate of energy generation within the control volume	W
\dot{E}_{out}	rate of energy leaving the system through the control volume	W
\dot{E}_{st}	rate of energy storage within the control volume	W
h	length of spherical cap	μm
h_{tot}	total heat transfer coefficient	$\text{W m}^{-2} \text{K}^{-1}$
k_b	Boltzmann constant	J K^{-1}
L	latent heat	kJ mol^{-1}
\dot{m}	mass reacting	kg s^{-1}
N	number of oxide entrainment cycles	
\bar{P}	coefficient in Eq 36	m^{-1}
P_{O_2}	oxygen partial pressure	torr
Q_e	energy of formation of the ion	eV
R	droplet radius	μm
Re_D	Reynolds number based upon droplet diameter	
s	wetted length	m
t	time	s
T_d	droplet temperature	K
T_{di}	droplet initial temperature	K
T_{∞}	ambient air temperature	K
v_s	average droplet surface velocity	m s^{-1}
v_0	droplet surface velocity along circumference of droplet	m s^{-1}
V_{rel}	relative velocity between droplet and air stream	m s^{-1}
V_d	droplet velocity	m s^{-1}
\mathcal{V}_d	volume of the spherical droplet	m^3
\mathcal{V}^{ox}	volume of the oxide shell	m^3
δ	oxide thickness	\AA
μ	dynamic viscosity	cp or N s m^{-2}
ρ	density	kg m^{-3}
θ	angle	degrees
φ	volume fraction of oxide in droplet	

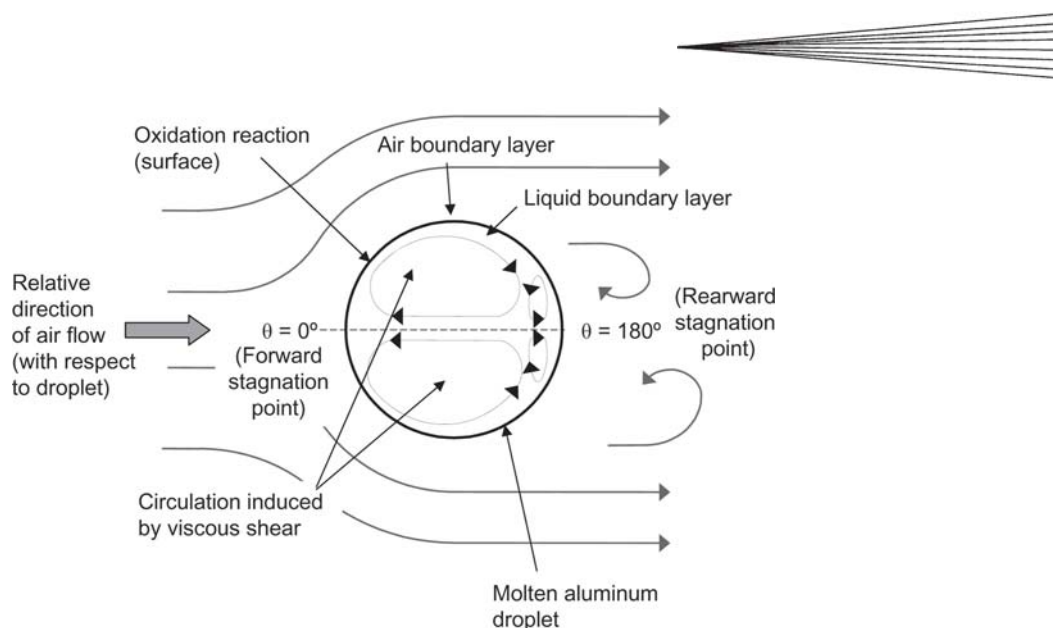


Fig. 1 Internal circulation within a fully molten droplet caused by shear forces from the high-velocity airflow around the droplet at a Reynolds number of 300

into the particle and mixed with the liquid aluminum by convective motion within the droplet. The internal circulation affects the amount of oxide in the droplets and, as a result, the as-sprayed coating. In contrast, a droplet without internal circulation (i.e., a solid particle) would form a continuous, self-limiting oxidation film on the droplet surface and the droplet would have a much lower oxide content.

4.1 Estimation of Droplet Surface Velocity

Numerical computations of the vortical flow within a raindrop falling at terminal velocity have been tabulated as a function of angle (position on the droplet surface) and flow Reynolds number by LeClair et al. (Ref 13). By comparing the results of the analyses to experimental data, they concluded that the viscous nature of the flow internal and external to the droplet played a significant role in the circulation patterns within the droplet. The internal circulation velocity is dependent upon the Reynolds number, relative velocity, and the viscosity ratio of the droplet and the freestream fluid. These data can be applied to the case of a molten metal droplet carried by an air stream to estimate the amount of aluminum oxide produced on the droplet surface and entrained into the droplet using an approach proposed by Neiser et al. (Ref 15).

From a boundary layer analysis, the droplet surface velocity is proportional to the dynamic viscosity ratio between the fluid external and internal to the droplet. To apply LeClair's data for the air/water system to the aluminum/air system, the nondimensional surface velocity for the air/water system is multiplied by the dynamic viscosity ratio for water and aluminum:

$$\left(\frac{v_{\theta}}{V_{\text{rel}}}\right)_{\text{Al}} = \left(\frac{v_{\theta}}{V_{\infty}}\right)_{\text{w}} \left(\frac{\mu_{\text{w}}}{\mu_{\text{Al}}}\right) \quad (\text{Eq 2})$$

LeClair's calculated variation of droplet surface velocity with angle, θ , over the surface of the droplet, v_{θ} , is nondimensionalized by the freestream velocity, V_{∞} , as the tabulated data consid-

ers raindrops falling through quiescent air in the reference frame of the moving droplet. However, the variation of droplet surface velocity with angle over the surface of the droplet, v_{θ} , for a thermal spray droplet is nondimensionalized by the relative velocity, V_{rel} , between the droplets and the air, as in the thermal spray problem considered here the droplets and air are both moving.

For water and air at standard conditions, the dynamic viscosity ratio is approximately 55, whereas for molten aluminum and air, the dynamic viscosity ratio is approximately 20. Using the principle of fluid dynamic similarity (Ref 16) and Eq 2, the velocities at the surface of the droplets are a factor of 2.75 larger for the liquid aluminum/air system. LeClair's numerical calculation of the variation of velocity at the surface of the droplet for a Reynolds number of 300 for a water/air system were scaled by this factor to account for the different dynamic viscosity ratio of the liquid aluminum/air system. Using LeClair's data for a Reynolds number of 300, which is applicable for a "typical" droplet under investigation, the flow reverses direction in the aft quadrant of the sphere. The nondimensionalized droplet surface velocity changes from a positive to negative at $\theta \approx 157.5^{\circ}$. The flow reversal entrains fluid into the core of the droplet via the main vortex, while oxide accumulates in the secondary vortex near the rear stagnation point of the liquid droplet where it is essentially trapped. The trapped oxides form an entrained oxide cap that has been reported at the tail of thermal sprayed particles (Ref 17).

Equation 2 was integrated to yield the average (rather than local) droplet surface velocity. The average droplet surface velocity, v_{s} , is a function of the relative velocity, V_{rel} , between the droplet and the air stream and the Reynolds number. The average droplet surface velocity and relative velocity are functions of axial distance along the spray plume, and thus also of time. However, for the "typical" droplet considered here, the average droplet surface velocity will be assumed constant throughout the droplet's flight. For a "typical" droplet traveling at a relative velocity of 140 m s^{-1} and with a Reynolds number of 300, the average droplet surface velocity, v_{s} , is 8.4 m s^{-1} .

4.2 Oxidation Mass Flow Rate Calculation

The rate of aluminum reacting at the surface of the aluminum droplet is analogous to a mass flow rate and can be calculated by the following expression:

$$\dot{m} = \int \rho_d \frac{d\delta}{dt} \cdot dA_{ox} \quad (\text{Eq 3})$$

where ρ_d is the droplet material density, $d\delta/dt$ is the rate of growth of the oxide layer, and A_{ox} is the oxidation area of the spherical droplet.

The surface area of the spherical droplet that oxidizes is dependent upon the droplet surface velocity. The oxide layer on the droplet surface builds until it reaches a maximum value, δ_{max} , which is dependent upon the size of the droplet (Ref 18). The oxidation reaction ceases when the insulating oxide layer becomes sufficiently thick to restrict the further tunneling of electrons from the metallic core (Ref 19). The time it takes for the oxidation layer to reach its maximum value, $t_{\delta_{max}}$, for a given droplet diameter can be calculated from the following expression:

$$t_{\delta_{max}} = \frac{\delta_{max}}{\left(\frac{d\delta}{dt}\right)} \quad (\text{Eq 4})$$

For a 39 μm droplet, δ_{max} is approximately 79 \AA (Ref 18). Therefore, applying Eq 1 and 4 to a “typical” aluminum droplet, $t_{\delta_{max}} = 1.51 \times 10^{-5}$ s. The time for one circulation cycle of oxide entrainment, t_{cycle} , is:

$$t_{cycle} = \frac{s}{v_s} = \frac{\pi D}{2v_s} = 7.293 \times 10^{-6} \text{ s} \quad (\text{Eq 5})$$

where s is the wetted length along the droplet surface and D is the droplet diameter. The time for one circulation cycle is defined here as the time for an oxide particle at the forward stagnation point of a “typical” droplet to travel along the droplet surface to the rear stagnation point. Note that $t_{\delta_{max}}$ and t_{cycle} are much less than the droplet time of flight, t_s .

The value of the droplet surface velocity at which the oxide layer will reach its limiting thickness at the rear stagnation point may be calculated as:

$$v_{s\delta_{max}} = \frac{s}{t_{\delta_{max}}} = \frac{\pi D}{2t_{\delta_{max}}} \quad (\text{Eq 6})$$

For a “typical” droplet, $v_{s\delta_{max}} = 4.1 \text{ m s}^{-1}$. Three cases are possible depending upon the relative values of v_s and $v_{s\delta_{max}}$:

- Case a. If $v_s < v_{s\delta_{max}}$, then the oxide layer thickness will reach its limiting value at a location along the droplet surface between the forward and rear stagnation points.
- Case b. If $v_s = v_{s\delta_{max}}$, then the oxide thickness will reach its maximum value at the rearward stagnation point.
- Case c. If $v_s > v_{s\delta_{max}}$, then the oxide layer will not reach its maximum value along the droplet surface.

The surface area available for oxidation, A_{ox} , is that of a spherical cap (Ref 20):

$$dA_{ox} = 2\pi R \int_0^h dh \quad (\text{Eq 7})$$

where h is the depth of the spherical cap and R is the droplet radius.

Integrating Eq 7 yields an expression for oxidation area as a function of droplet radius and internal circulation velocity:

$$A_{ox} = 2\pi R^2 \left[1 - \cos\left(\frac{v_s t_{\delta_{max}}}{R}\right) \right] \text{ for } t_{\delta_{max}} < t_{cycle} \quad (\text{Eq 8})$$

$$A_{ox} = A \text{ for } t_{\delta_{max}} \geq t_{cycle} \quad (\text{Eq 9})$$

where A is total droplet surface area. Equation 8 is applicable for the oxidation over a portion of the droplet surface and corresponds to Case a. Equation 9 corresponds to Cases b and c, where the entire surface area of the droplet oxidizes.

A “typical” droplet corresponds to Case c, because $t_{\delta_{max}} > t_{cycle}$. The oxide thickness at the rear stagnation point will grow to a thickness of 38 \AA in one circulation cycle, as can be calculated by the following expression:

$$\delta_{cycle} = \left(\frac{d\delta}{dt}\right) t_{cycle} \quad (\text{Eq 10})$$

This oxide thickness is less than the limiting value of 79 \AA for a 39 μm droplet. This calculated value is within the expected range of oxide thicknesses of one to a few hundred angstroms (Ref 21).

For a given droplet size, temperature, and freestream oxygen content, the oxidation area is the only variable in Eq 3 that changes. This analysis shows that the rate of mass reacting is dependent upon oxidation area, which is a function of both droplet diameter and surface velocity. It was shown in the previous subsection that droplet surface velocity is a function of the relative velocity between the droplet and the air stream and the Reynolds number.

5. Oxide Content Calculation

Consider the oxide layer build up on the surface of the droplet, the growth of which is limited similar to that of a solid particle. A solid particle forms a continuous, self-limiting oxidation film that serves as a barrier to further oxidation of the droplet surface. The oxide volume fraction for a solid spherical particle with an oxide shell, ϕ_{solid} , can be calculated by:

$$\phi_{solid} = \frac{V_{ox}}{V_d} \quad (\text{Eq 11})$$

where V_d is the volume of a sphere and V_{ox} is the volume of an oxide shell on the outer surface of the sphere.

For a droplet with internal circulation, the volume fraction, ϕ_{circ} , is expressed as:

$$\phi_{circ} = \frac{V_{ox}N}{V_d} \quad (\text{Eq 12})$$

The number of circulation cycles, N , is defined as the time of flight for a droplet divided by the time required for one circulation cycle:

$$N = \frac{t_s}{t_{\text{cycle}}} \quad (\text{Eq 13})$$

5.1 Oxide Content in a “Typical” Droplet

The oxide content in a solid spherical particle will be estimated first and then be compared to that of a droplet with internal circulation. For aluminum powder formed by atomization in air, the mean oxide thickness, δ , on the surface of a 39 μm particle grows until it reaches a maximum thickness, δ_{max} , of 79 \AA (Ref 18). From Eq 11, the volume fraction of oxide for a solid spherical particle, φ_{solid} , is 0.0012 or 0.12%. This calculated oxide volume fraction correlates well to the oxygen content of 0.116% for commercially produced aluminum powders (Ref 18). When aluminum powders are manufactured, the powder particles are typically quenched immediately to minimize the formation of aluminum oxide so that the powder will be as pure as possible.

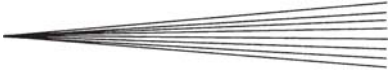
For a “typical” droplet with internal circulation, there are approximately 148 cycles of oxide build up and entrainment into the droplet. From Eq 10, the oxide thickness at the rear stagnation point will build up to a thickness, δ_{cycle} , of 38 \AA in each cycle. Using Eq 12, the volume fraction of oxide produced during the entire flight for a “typical” droplet with internal circulation, φ_{circ} , is calculated to be 0.087 or 8.7%. In contrast to a solid particle, the oxide volume fraction computed for a droplet with internal circulation is nearly two orders of magnitude larger. This dramatic difference in oxide volume fraction reinforces the hypothesis that internal circulation is a significant mechanism for oxide production within the droplet.

5.2 Effect of Altitude on Oxide Content

From Eq 1, it can be seen that the rate of growth of the oxide layer is highly sensitive to the oxygen content of the ambient air. Therefore, the altitude at which the spraying is performed affects the amount of oxide produced in the droplet. It is important to point out that the spray plume experiments and the coating fabrication were conducted at laboratories at the same elevation. The oxide content of the coating could be increased by performing the spraying operations at a lower altitude, where the atmospheric pressure (and thus the oxygen partial pressure) is higher. Conversely, the oxide content of the coating could be decreased by performing the spraying at a higher altitude. The theoretical maximum oxide content in a “typical” droplet at a pressure of 1 atm may be calculated assuming that the oxide layer thickness reaches a maximum of 79 \AA per circulation cycle. The theoretical maximum oxide content of a “typical” droplet sprayed at sea level is therefore approximately 18.0%. This calculated maximum oxide content is more than double the oxide content produced at the laboratory elevation of 4500 ft (1372 m) above sea level.

5.3 Relationship Between Droplet and Coating Oxide Content

Calculations of oxide content in a “typical” droplet can be compared with experimental data on the oxide content in a typi-



cal thermal spray coating. The thermal spray flowfield consists of a polydisperse distribution of droplets. A “typical” droplet is representative of all droplets in the flowfield, because a coating is effectively created by an ensemble of droplets impacting on a substrate. Thus, the “typical” droplet oxide volume fraction can be related to the oxide content of the coating measured at multiple cross sections and then averaged. Because oxides are formed both during droplet flight and during deposition on a substrate, the amount of oxides in the droplets must be less than the oxide content of the coating. The oxide content calculated for a “typical” droplet correlates well with the experimentally determined oxide content in TWEA-sprayed aluminum coatings obtained by Varacalle et al. (Ref 22), which ranges from 3.3 to 12.7%.

Experiments by Varacalle et al. (Ref 22 and 23) showed that coatings with the minimum oxide content were produced at the shortest standoff distance. This can be explained since at shorter standoff distances there is less time available for the continual oxidation caused by internal circulation in the droplets during flight. A key factor to determining the amount of oxide produced within the liquid droplets is the number of circulation cycles. Varacalle’s coatings were produced on room temperature substrates rather than heated substrates, which minimized the time for oxidation after impact. The calculations of droplet oxide content compare favorably to the experimentally measured oxide content in these coatings. This result supports the hypothesis that internal circulation within the droplets during flight is a major contributor to the oxide content of the coating. This conclusion is also supported by experimental data in the literature. Auger spectroscopy and ion milling data of solidified iron and aluminum splats reveal that most of the oxidation occurs prior to impact (Ref 15 and 24).

6. Heat Transfer Effect

Computational fluid dynamic predictions by other researchers showed that the droplets would initially oxidize and then form a protective oxide layer that would serve as a barrier to further oxidation. Their results indicated that the droplets would then cool throughout their flight through the air and could even solidify prior to impact (Ref 25). This is contrary to the in-flight experimental observations that revealed highly superheated droplets with nearly constant temperature throughout their flight. Thus, a mathematical explanation for this discrepancy was sought.

The energy balance at the surface of the in-flight droplet is given by the following equation representing conservation of energy for a control volume:

$$\dot{E}_{\text{in}} - \dot{E}_{\text{out}} + \dot{E}_{\text{g}} = \dot{E}_{\text{st}} \quad (\text{Eq 14})$$

where \dot{E}_{in} is the rate of energy entering the system through the control volume, \dot{E}_{out} is the rate of energy leaving the system through the control volume, \dot{E}_{g} is the rate of energy generation within the control volume, and \dot{E}_{st} is the rate of energy storage within the control volume. In this problem, the energy entering the system, \dot{E}_{in} , is set to zero.

The energy generation term due to the combined effects of

the surface oxidation reaction and the latent heat release due to solidification of the aluminum oxide layer is represented as:

$$\dot{E}_g = \dot{m}(\Delta H_f + L) \quad (\text{Eq 15})$$

where ΔH_f is the heat of formation of aluminum oxide and L is the latent heat release due to solidification of aluminum oxide. Because the temperature of a “typical” droplet is slightly below the solidification temperature of aluminum oxide, the latent heat term is accounted for in Eq 15. However, the latent heat contribution is only 6.2% of the total heat generation.

The rate of energy leaving the control volume, \dot{E}_{out} , is composed of convection and a radiation term. Newton’s law of cooling is used to estimate the heat convected from the molten droplet (Ref 26), with the convection heat transfer coefficient calculated using the Ranz-Marshall correlation (Ref 27). The radiation term is expressed using Stefan’s law (Ref 28) with the emissivity of aluminum oxide at the average surface temperature. The sum of the convection and radiation heat transfer coefficients is expressed as a total heat transfer coefficient, h_{tot} . Using an emissivity value, ϵ , of 0.16 for aluminum oxide at 2273 K (Ref 29), the magnitude of the radiation heat transfer coefficient is only 1.2% of the total heat transfer coefficient. Convection is the dominant mode of heat loss from the system.

The rate of energy storage within the control volume is given by:

$$\dot{E}_{st} = \rho_d c_p V_d \frac{dT_d}{dt} \quad (\text{Eq 16})$$

where ρ_d is the droplet material density, c_p is the specific heat of droplet material, and dT_d/dt is the time rate of change of temperature of the droplet. The lumped capacitance assumption was used to calculate the transient droplet temperature because the Biot number, Bi , is small (i.e., $Bi < 0.1$), which means that the temperature distribution within the molten droplet can be considered uniform (Ref 26). The rate of change of droplet temperature is obtained by solving for dT_d/dt .

Because droplet temperature data are available as a function of axial distance along the spray plume, rather than time, it is desirable to integrate with respect to x rather than t . This can be accomplished by expressing (Ref 30):

$$\frac{dT_d}{dt} = \frac{dT_d}{dx} \cdot \frac{dx}{dt} \quad (\text{Eq 17})$$

and making the following substitution

$$\frac{dx}{dt} = V_d \quad (\text{Eq 18})$$

where V_d is the droplet velocity.

The solution of the resulting first-order differential equation is (Ref 31):

$$T_d(x) = e^{-\bar{P}x} \left[T_{di} + \frac{\bar{Q}}{\bar{P}} (e^{\bar{P}x} - 1) \right] \quad (\text{Eq 19})$$

where

$$\bar{P} = \frac{h_{tot}A}{\rho_d c_p V_d V_d}$$

$$\bar{Q} = \frac{1}{\rho_d c_p V_d V_d} \dot{E}_g + \frac{h_{tot}AT_\infty}{\rho_d c_p V_d V_d}$$

In Eq 19, T_{di} is the initial droplet temperature and T_∞ is the ambient air temperature. \bar{P} and \bar{Q} were evaluated using air properties at a film temperature of 1285.5 K, aluminum properties at 2273 K, an ambient air temperature of 293 K, and the kinematic viscosity for air at the laboratory elevation. To match the experimental data, an initial droplet temperature of 2336 K was chosen. Temperature predictions using Eq 19 for a “typical” droplet with heat generation closely match the experimental data. From the axial location of 22 to 177 mm, the calculated temperature drop is 100 K versus a measured temperature drop of 92 K.

If the energy generation term is neglected, a simplified differential equation is obtained. The solution of the governing differential equation becomes:

$$T_d(x) = T_\infty + (T_{di} - T_\infty)e^{-\bar{P}x} \quad (\text{Eq 20})$$

To calculate the value of \bar{P} in Eq 20, a new value of the convection heat transfer coefficient was computed using air properties at a film temperature of 1088 K. Aluminum and aluminum oxide properties at an average droplet temperature, T_d , of 1878 K were used to specify material properties. If the energy generation term is neglected in the surface energy balance equation, the temperature of a “typical” droplet is calculated to decrease by approximately 1045 K over a distance of 178 mm (5 in.).

Numerical calculations by Varacalle et al. (Ref 25) using a computer code in the TEACH family of codes developed by Zhou and Yao (Ref 32) predict that the smaller droplets may actually solidify before impact (depending upon standoff distance). Varacalle’s computational fluid dynamic results show the droplet temperature for a 39 μm molten aluminum droplet decreases by approximately 1450 K from an initial temperature of 2400 K over a distance of 178 mm. Varacalle et al. (Ref 25) accounted for the initial oxidation of the molten aluminum droplets in the initial droplet temperature but did not consider the continual generation of heat due to the oxidation reaction caused by the internal circulation within the molten droplet.

Figure 2 compares the transient temperature profiles of the experimental measurements, the predicted droplet temperature with and without the continual heat generation term, and Varacalle’s results. The importance of including the heat generation from the oxidation reaction as a continual source term in the energy balance is clearly demonstrated.

The analysis performed using the first order linear differential equations given by Eq 19 and 20 considered a “typical” droplet traveling along the plume centerline. Droplet temperatures predicted by Varacalle et al. (Ref 25) are lower than the predictions obtained using Eq 20. This is attributed to the fact that the droplet clusters used in the computations did not remain along the plume centerline during flight. As the droplets move radially outward from the plume centerline, they reside in the plume longer, which provides more time for convective cooling to occur.

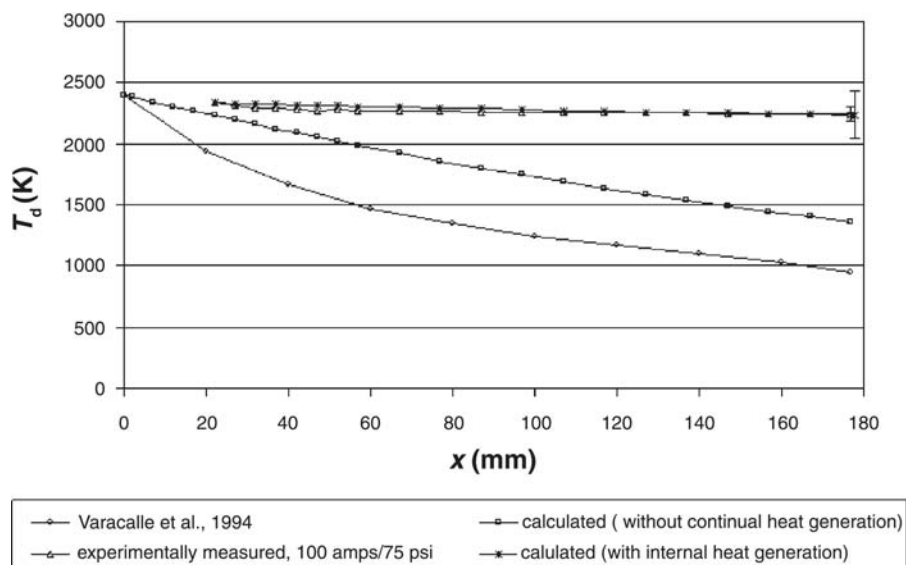


Fig. 2 Comparison of droplet temperatures along spray plume centerline, with and without internal heat generation

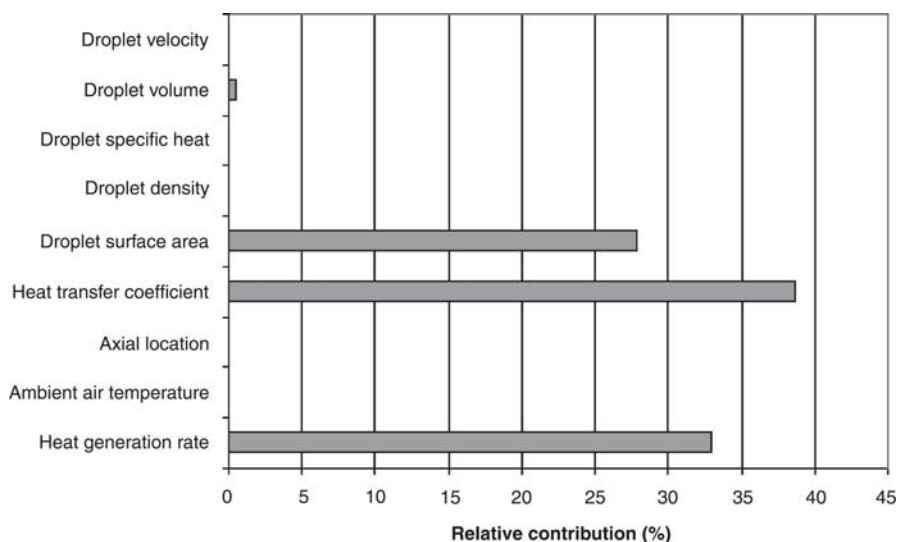


Fig. 3 Pareto chart for uncertainty in temperature calculation

7. Uncertainty Analysis

An uncertainty analysis was performed to estimate the relative contribution of relative errors from various sources in the analyses (Ref 33). The total combined uncertainty of the calculated droplet temperature is 395 K or 17.4%. The uncertainty of the measurements and calculations are indicated by error bars in Fig. 2. In Fig. 2, the uncertainties overlap between the experimentally measured droplet temperatures and the droplet temperatures calculated using the governing differential equation for a droplet with internal circulation.

The Pareto chart shown in Fig. 3 displays a bar chart that ranks the relative contribution of individual uncertainties to the total combined uncertainty. The most effective approach to decrease the error in the overall analysis is to reduce the uncer-

tainty contributions from the terms with the largest relative contribution. In the calculation of droplet temperature, reducing the error in the heat transfer coefficient, heat generation rate, and droplet surface area, respectively, would have the greatest effect. The uncertainty contribution of the other variables is negligible.

The uncertainty of the oxide content calculation is ± 0.0496 . Because the calculated value for oxide content of a “typical” droplet is calculated to be 0.087, the range of estimated oxide content is therefore 0.0370-0.1362 or 3.7-13.6%. This correlates well to the measured coating oxide content of 3.3-12.7%.

Figure 4 compares the relative uncertainty contributions from the calculated oxide volume, number of circulation cycles, and the droplet volume. The Pareto chart shows that improving the uncertainty in droplet volume (i.e., droplet diameter) will

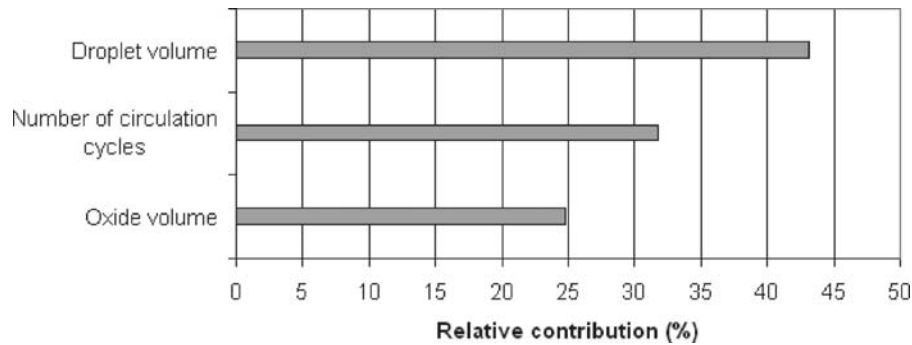


Fig. 4 Pareto chart for uncertainty in oxide content calculation

have the greatest effect on the uncertainty. As the number of circulation cycles and the oxide volume are also significant contributors to total combined uncertainty, and these quantities are also dependent upon droplet diameter, reducing the uncertainty in droplet diameter would serve to reduce the uncertainty in the calculated oxide content of the droplet.

8. Summary and Conclusions

The effects of toroidal flow within a “typical” TWEA-sprayed aluminum droplet on the droplet temperature and oxide content were evaluated mathematically and compared with experimental data. The fluid dynamics and heat transfer of the droplet are driven by the relative velocity between the droplets and the air stream. Aerodynamic shear serves as the driving mechanism to continually sweep fresh fluid to the droplet surface, where it is then available for oxidation. The oxidation reaction takes place during the flight of the droplet to the substrate due to the continual resupply of liquid aluminum to the droplet surface. This phenomenon explains the fact that the experimentally measured droplet temperatures (~2273 K) were much higher than the melting point for aluminum (933 K) and remained near this temperature throughout their flight to the substrate. Results of the transient heat transfer analysis incorporating continual heat generation predict a temperature drop of 100 K, which is in excellent agreement with the experimentally measured temperature drop of 92 K.

To estimate droplet oxide content of the aluminum droplets in the TWEA process, data on the internal circulation within raindrops falling at terminal velocity tabulated by LeClair et al. (Ref 13) was scaled to estimate droplet surface velocity. A 39 μm aluminum droplet traveling with a relative velocity of 140 m s^{-1} and a constant temperature of 2273 K was used to represent a “typical” droplet. Oxide entrainment in a “typical” droplet due to internal circulation was found to produce an oxide volume fraction nearly *two orders of magnitude* greater than that of a solid particle. The estimated oxide volume fraction of 8.7% for a droplet with internal circulation correlates well with the experimentally measured average oxide content in a typical TWEA-sprayed aluminum coating microstructure, which ranges from 3.3 to 12.7%. By operating the TWEA process at sea level, rather than at the 4500 ft (1372 m) laboratory altitude, the oxide content of a “typical” droplet could theoretically be nearly doubled.

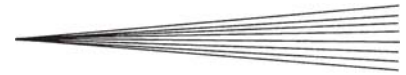
Conversely, it is expected that spraying operations conducted at higher altitudes will result in a lower coating oxide content.

Acknowledgments

This paper was authored by Battelle Energy Alliance, LLC, under Contract No. DE-AC07-05ID14517 with the U.S. Department of Energy.

References

1. W.A. Sirignano, *Fluid Dynamics and Transport of Droplets and Sprays*, Cambridge University Press, 1999
2. D.L. Hale, D.W. Swank, and D.C. Haggard, In-Flight Particle Measurements of Twin Wire Electric Arc Sprayed Aluminum, *J. Thermal Spray Technol.*, 1998, 7 (1), p 58-63
3. R.N. Lyon, *Liquid-Metals Handbook*, 2nd ed., The Committee on the Basic Properties of Liquid Metals and The Office of Naval Research, Department of the Navy, U.S. Government Printing Office, Washington, DC, 1952, p 40-45
4. L. Bretherick, *Handbook of Reactive Chemical Hazards*, 3rd ed., Butterworth and Co., London, 1985
5. O. Kubaschewski and B.E. Hopkins, *Oxidation of Metals and Alloys*, 2nd ed., Butterworth and Co., London, 1967, p 71
6. Y.P. Wan, J.R. Fincke, X.Y. Jiang, S. Sampath, V. Prasad, and H. Herman, Modeling of Oxidation of Molybdenum Particles during Plasma Spray Deposition, *Metall. Mater. Trans. B*, 2001, 32B, p 475-481
7. N. Cabrera and N.F. Mott, Theory of the Oxidation of Metals, *Rep. Progr. Phys.*, 1948, 12, p 163-184
8. S.L. Dai, J.-P. Delplanque, and E.J. Lavernia, Microstructural Characteristics of 5083 Al Alloys Processed by Reactive Spray Deposition for Net-Shape Manufacturing, *Metall. Mater. Trans. A*, 1998, 29A, p 2597-2611
9. M.J.M. Hill, On a Spherical Vortex, *Phil. Trans. R. Soc.*, 1894, 185, p 213-245
10. G.K. Batchelor, On Steady Laminar Flow with Closed Streamlines at Large Reynolds Number, *J. Fluid Mech.*, 1958, 1, p 177-190
11. J.F. Harper and D.W. Moore, The Motion of a Spherical Liquid Drop at High Reynolds Number, *J. Fluid Mech.*, 1968, 32, p 367-379
12. S. Prakash and W.A. Sirignano, Liquid Fuel Droplet Heating with Internal Circulation, *Int. J. Heat Mass Transfer*, 1978, 21, p 885-895
13. G.P. LeClair, A.E. Hamielec, H.R. Pruppacher, and W.D. Hall, A Theoretical and Experimental Study of the Internal Circulation in Water Drops Falling at Terminal Velocity in Air, *J. Atmos. Sci.*, 1972, 29, p 728-740
14. L. Melton, “Experimental Methods for CFD Evaluation,” presentation at *Computational Fluid Dynamics in Chemical Reaction Engineering VII*, Quebec, Canada, August 2000
15. R.A. Neiser, M.F. Smith, and R.C. Dykhuizen, Oxidation in Wire HVOF-Sprayed Steel, *J. Thermal Spray Technol.*, 1998, 7 (4), p 537-545
16. R.L. Daugherty, J.B. Franzini, and E.J. Finnemore, *Fluid Mechanics*



- with *Engineering Applications*, 8th ed., McGraw-Hill, Inc., New York, 1985
17. H. Ageorges and P. Fauchais, Plasma Spraying of Stainless Steel Particles Coated with an Alumina Shell, *Thin Solid Films*, 2000, 370, p 213-222
 18. Properties and Selection, *Nonferrous Alloys and Special-Purpose Materials*, Vol 2, *ASM Handbook*, ASM International, 1991
 19. J. Xu, and C.P. Wong, Low-Loss Percolative Dielectric Composite, *Appl. Phys. Lett.*, 2005, 87 (8), article no. 082907
 20. J.W. Harris and H. Stocker, Spherical Segment (Spherical Cap), *Handbook of Mathematics and Computational Science*, §4.8.4, Springer-Verlag, 1998, p 107
 21. J.-P. Delplanque, E.J. Lavernia, and R.H. Rangel, Analysis of In-Flight Oxidation During Reactive Spray Atomization and Deposition Processing of Aluminum, *Transactions of the ASME*, Vol 122, ASM International, February 2000, p 126-133
 22. D.J. Varacalle Jr., R. Mizia, C. Shelton-Davis, L. Torres, V. Zanchuck, and E. Sampson, Twin-Wire Electric Arc Sprayed Zinc and Aluminum Coatings, *Proceedings of the SSPC 1996 Seminars, Technologies for a Diverse Industry*, Charlotte, NC, 17-21 November 1996, p 137-143
 23. D.J. Varacalle, Jr., D.P. Zeek, V. Zanchuck, E.R. Sampson, K.W. Couch, D.M. Benson, and G.S. Cox, "Use of Thermal Spray Processes for Refurbishing TRU Waste Containers," *1998 Waste Management Symposia*, Tucson, AZ, 1-5 March 1998
 24. M.F. Smith, R.C. Dykhuizen, and R.A. Neiser, Oxidation in HVOF-Sprayed Steel, *Proceedings of the 10th United Thermal Spray Conference*, Indianapolis, IN, 1997, p 885-893
 25. D.J. Varacalle Jr., G.C. Wilson, R.W. Johnson, T.J. Steeper, G. Irons, W.R. Kratochvil, and W.L. Riggs, A Taguchi Experimental Design Study of Twin-Wire Electric Arc Sprayed Aluminum Coatings, *J. Thermal Spray Technol.*, 1994, 3 (1), p 69-74
 26. J.P. Holman, *Heat Transfer*, 9th ed., McGraw-Hill, 2002, p 134-135, 221
 27. W.E. Ranz and W.R. Marshall Jr., Evaporation from Drops, *Chem. Eng. Prog.*, 1952, 48 (3), p 141-146
 28. R. Siegel and J.R. Howell, *Thermal Radiation Heat Transfer*, Hemisphere Publishing Company, New York, 1992
 29. K. Wefers and C. Misra, *Oxides and Hydroxides of Aluminum*, Alcoa Laboratories, Pittsburgh, PA, 1987, p 18-23
 30. D.T. Greenwood, *Principles of Dynamics*, Prentice-Hall, Inc., 1965, p 72
 31. I.S. Gradshteyn and I.M. Ryzhik, *Table of Integrals, Series, and Products*, 6th ed., Academic Press, 2000, p 1086
 32. W. Zhou and S.C. Yao, A Group Model for Particle Dispersion in Turbulent Sprays, *Heat and Mass Transfer in Fires and Combustion Systems*, HTD-148, American Society of Mechanical Engineers, 1990, p 27-32
 33. B.K. Hodge and R.P. Taylor, *Analysis and Design of Energy Systems*, 3rd ed., Prentice Hall, Inc., 1999, p 396-419